Development and Verification of a Monte Carlo Dose Calculation Program MagicDose for Boron Neutron Capture Therapy[*]

Ai-Kou Sun,[1,2] Zhen-Ping Chen,[1,2,3,†] Ke-Kun Gao,[2] Lin Zhu,[1,2] Cheng-Wei Liu,[1,2] Zhi-Qiang Wu,[4] Chao Yang,[1,2] Tong Liu,[5] Song Wang,[5] Zi-Zhu Zhang,[5,6] Yi-Zheng Chong,[7] and Tao Yu[1,2,‡]

[1]*School of Nuclear Science and Technology, University of South China, Hengyang, Hunan 421001, China*
[2]*Key Lab of Advanced Nuclear Energy Design and Safety,*
Ministry of Education, Hengyang, Hunan 421000, China
[3]*State Key Laboratory of Radiation Medicine and Protection, Soochow University, Suzhou, Jiangsu 215123, China*
[4]*Graduate School of Biomedical Engineering, Tohoku University, Sendai, Japan*
[5]*Beijing Capture Technology Co.Ltd, Beijing 102413, China*
[6]*Beijing Nuclear Industry Hospital, Beijing 102413, China*
[7]*China National Nuclear Corporation Overseas Ltd, Beijing 100044, China*

Dose calculation is the foundation of Boron Neutron Capture Therapy (BNCT). MagicDose, a dose calculation program for the BNCT treatment planning system, is developed based on the Monte Carlo method. Firstly, the voxel phantom of the modified Snyder head with 16, 8 mm are constructed, and the deviation of each result on *y=x* and the calculation time are statistical. The modified Snyder head phantom with tumor at three different spatial resolutions of 16, 8, and 1 mm are constructed, and the depth-dose-rate curves and spatial distribution maps are analyzed. Finally, the patient's head CT data is used as an application. The results show that the results calculated by MagicDose and MCNP are in good consistency, demonstrating that the computational efficiency of MagicDose is also better than that of MCNP. As the spatial resolution increases, the variability of the dose rate results is smaller. The voxel size and the number of threads are both inversely proportional to the time. For the CT model, the voxel phantom is successfully constructed and the calculation results are reasonable. The above results verify the correctness of MagicDose, which also provides a reference for optimizing the design of the voxel phantom in clinical treatment.

Keywords: Boron neutron capture therapy (BNCT), Monte Carlo, Dose calculation, MCNP, Voxel phantom, Spatial resolution

I. INTRODUCTION

Cancer has now become the leading cause of death around the world. According to GLOBOCAN 2020 global cancer statistics, there will be 4.82 million new cancer patients and 2.57 million deaths in China in 2022 [1], and it is a major problem affecting national health. Currently, cancer treatment modalities include mainly surgery, chemotherapy, and radiation therapy, and almost 50% to 70% of cancer patients in China will receive radiation therapy during treatment, and radiotherapy has been playing an increasingly important role in cancer treatment. Among them, Boron Neutron Capture Therapy (BNCT), as a state-of-the-art tumor radiotherapy technology based on neutron radiotherapy, has been developed in various countries around the world. Its main principle is to inject boron-containing drugs (Boronophenylalanine, BPA; Sodium Boronophenylalanine, BSH) with tumor specificity into the patient's body. After a period of metabolism of the boron drug in the patient's body, the drug will be enriched in the tumor area and then the tumor will be irradiated with the neutron beam generated by the neutron source. Due to the abnormally large thermal neutron absorption cross-section of ^{10}B, a large amount of ^{10}B will undergo the ^{10}B(n,α)^{7}Li reaction, which will release two high Linear Energy Transfer (LET) particles - α and ^{7}Li. Through these two particles, energy will be deposited in a range of approximately 12-13 μm, causing irreparable damage to cellular DNA in the area of deposited energy, and ultimately killing tumor cells [2]. The BNCT reaction formula and the basic schematic diagram are shown in Fig. 1.

BNCT treatment consists of the calculation and analysis of the distribution of irradiation doses in the patient's body, which is used to determine the optimal treatment plan for the duration and angle of orientation of the neutron beam exposure while observing the dose limitations that jeopardize normal tissues and organs. The tissue dose in BNCT consists of the following four parts [3]:

(1) Boron dose. It is produced by the ^{10}B(n,α)^{7}Li reaction, and because the absorption cross-section of boron for thermal neutron is very large (3840b), the reaction releases much energy, thus the boron dose contributes a lot to the total dose and is the main part.

(2) Thermal neutron dose. The thermal neutron reacts with the ^{14}N atom in the human body to generate recoil nuclei ^{14}C and a proton, and the dose is generated by the deposition of energy in cells in the human body.

(3) Epithermal and fast neutron dose. Statistics of the energy deposited by elastic scattering of all neutrons except the thermal neutron.

(4) Photon dose. There are three main production pathways, γ-ray produced by the accompanying incident neutron

$$^{10}_{5}B + ^{1}_{0}n \rightarrow ^{11}_{5}B^{*} \begin{cases} ^{7}_{3}Li + ^{4}_{2}He + 2.79\,Mev & (6.1\%) \\ ^{7}_{3}Li + ^{4}_{2}He + 2.31\,Mev & (93.9\%) \\ \downarrow \\ ^{7}_{3}Li + \gamma + 0.478\,Mev \end{cases}$$

(a)

Neutron beam

Nuclear reaction

Neutron beam

Normal cell

Tumor cell

Boron medicine

Neutron beam

Alpha particle   Lithium recoilion

γ ray

(b)
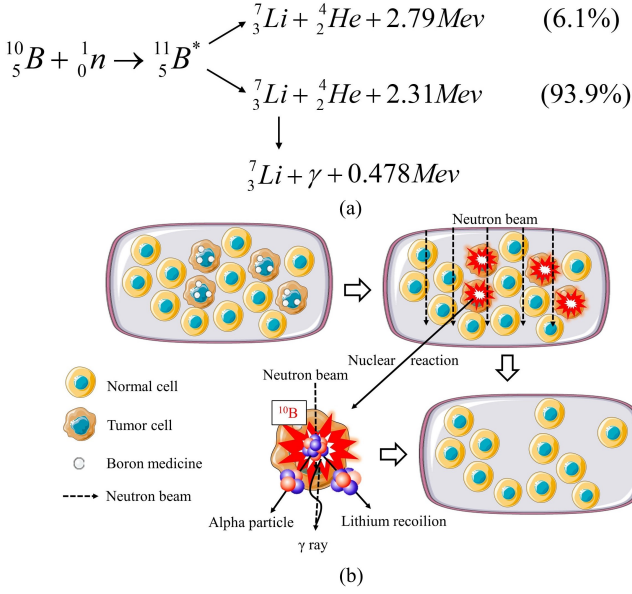
Fig. 1. **(a)** ^{10}B(n,α)^{7}Li reaction formula; **(b)** BNCT schematic diagram.

beam, ray produced in the boron neutron capture reaction, and γ-ray produced by the thermal neutron capture reaction with the H atom in the human body.

The calculations of the four dose components above are very complicated, and there is no empirical formula for accurate dose calculation. At this stage, the Monte Carlo (MC) simulation is used mainly in the BNCT Treatment Planning System (TPS) to calculate the radiation dose distribution of patients. Moreover, the TPS of BNCT is significantly different from the photon or electron TPS of conventional radiotherapy. In conventional radiotherapy, only a single dose from the primary photon or electron needs to be calculated, and a simple numerical model-based approach is applied to accelerate the calculation. For the calculation of the dose of BNCT, many factors are involved such as the neutron source, the boron content, the distribution of the neutron energy in tissues, and the total dose composed of different doses with different biological effects, which makes its TPS more complicated compared to traditional methods and requires greater accuracy and technical support to ensure the effectiveness and safety of treatment. Currently, international TPS technology for BNCT is becoming mature, and a variety of BNCT treatment software has been developed, mainly including NCTPlan and SERA in the United States [4, 5], BDTPS in Italy [6], JCDS-FX, TsukubaPlan and NeuCure in Japan [7–9], and NeuMANTA, THORPlan and MCDB in China [10–12]. The characteristics of each BNCT treatment planning system are shown in TABLE 1.

The TPS of BNCT consists of three parts: pre-processing, post-processing, and dose calculation (Fig. 2), in which the pre-processing is used to read and display the CT/MRI medical image data (including the body geometry and material), and cooperates with the neutron irradiation conditions to generate the input file required for dose calculation; the post-processing will process the output of the dose calculation and display the results in graphs, which is convenient for the users to analyze the results of the calculation; the dose calculation is the core part of the whole TPS, and the MC method is usually used to simulate the dose of particles produced by neutron beam. As can be seen from TABLE 1, the MCNP has been widely used as the TPS dose calculation program for BNCT because it supports neutron-photon multiparticle simulation, is relatively easy to use, provides flexible source definitions, has a large number of users, and has been fully validated by experiments. However, the MCNP program system is too enormous, and it is limited not only to the application in the field of nuclear medicine but also to the fields of nuclear energy, nuclear engineering and nuclear technology, and other related theoretical calculations. At the same time, MCNP, as commercial software, is subject to strict licensing restrictions, especially in certain countries (e.g., China) or specific application areas, and Fortran programming has weak support for object-oriented programming, which is not as comprehensive and flexible as C++ and is not conducive to the subsequent development of specific areas of needs. Therefore, a program specifically for dosimetry computation in BNCT is needed, which should be characterized by a small program size, a high degree of autonomy, and friendly extensibility.

In this paper, based on the Monte Carlo particle transport method and C++, MagicDose, a dedicated dose calculation program for the BNCT treatment planning system, is developed independently. Compared with MCNP, it has a small program size, strong specialization, and high degree of autonomy, while adopting a module design, which makes the various functional modules of the program can be developed and maintained independently, and facilitates the secondary development of BNCT's subsequent demands. It provides specific functions such as fine-voxelization phantom construction, human tissue composition material library, Kerma (Kinetic Energy Released in Matter) factor library, spatial plane rotation, and translation source term for the needs of BNCT dose calculation, etc. Meanwhile, it supports server parallel computing and results visualization, so that users can analyze the results intuitively in a shorter time. In order to test and validate the developed MagicDose program, this paper based on MagicDose: (1) Firstly, the study prepare the voxel phantom of modified Snyder head with 16,8 mm resolution as a benchmark problem, and verified that under the same irradiation conditions, the neutron and photon dose rate values calculated by MagicDose and MCNP are consistent and that MagicDose outperforms MCNP in terms of computational efficiency; (2) Then, on the basis of verifying the correctness of the procedure, in order to explore the influence of the voxel phantom on the calculation results under different spatial resolutions, MagicDose combines with the material-located method with the central point algorithm to construct the voxel phantom of modified Snyder head with tumor with three different spatial resolutions of 16, 8, and 1 mm, and analyzes the influence of the model voxel sizes on the calculation results by the results of the depth-dose-rate curves and spatial value distribution maps. At the same time, the parallel computational efficiency of MagicDose is analyzed and the computational time

TABLE 1. Characteristics of the international BNCT treatment planning system. [13, 14]

| TPS	Country/Institution	Geometry	Dose program	Cross section
NCTPlan	USA/Harvard-MIT	voxel	MCNP4B/5	continuous energy
SERA	USA/INEEL-MSU	univel	seraMC	multigroup
BDTPS	Italy/University of Pisa/JRC	voxel	MCNP	continuous energy
JCDS-FX	Japan/JAEA	voxel/multi-voxel	MCNP5	continuous energy
TsukubaPlan	Japan/Tsukuba University	voxel	PHITS	continuous energy
NeuCure	Japan/Sumitomo Heavy Industry	voxel	PHITS	continuous energy
NeuMANTA	China/Neuboron	voxel	COMPASS	continuous energy
THORPlan	China/Tsing Hua University	voxel	MCNP4C	continuous energy
MCDB	China/IAPCM,Beijing	voxel	MCNP4C	continuous energy
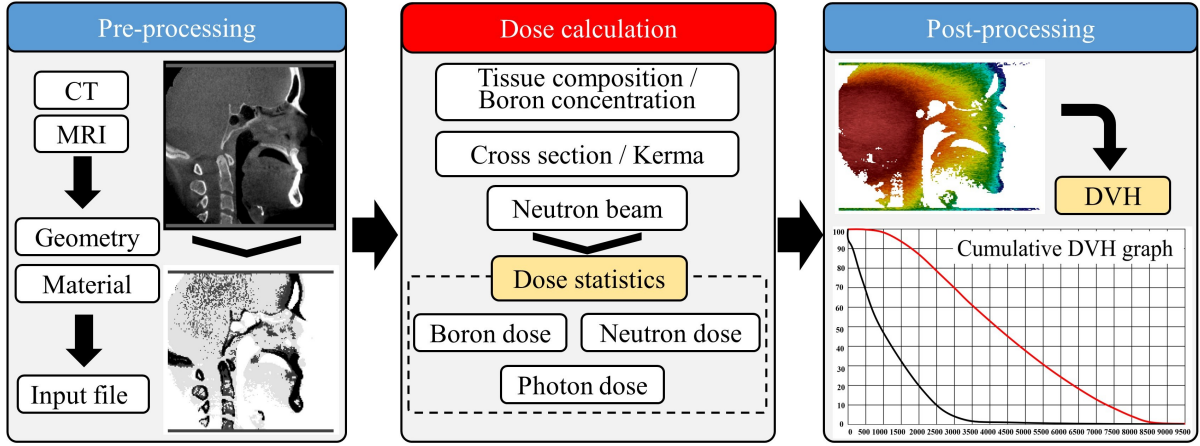
Fig. 2. BNCT-TPS.

is calculated at different spatial resolutions and the number of threads is calculated; (3) Finally, based on the CT head model of a patient, MagicDose is initially applied to a clinical case of BNCT.

II.   MATERIAL AND METHOD

A.   MagicDose program development & framework

Dose calculation is the core part of the whole BNCT treatment planning system, and in this paper, based on the Monte Carlo particle transport method, MagicDose, a dose calculation program dedicated to the BNCT treatment planning system, is developed in C++, which is convenient for future development and maintenance of the BNCT treatment planning system. MagicDose program consists of seven functional modules, including Geometry module, Source module, Database module, Particle Transport module, Tally module, Output module, and Auxiliary module. Fig. 3 shows the MagicDose development framework.

(1) Geometry module: In the BNCT treatment planning system, the 3D voxel phantom is the most commonly used geometric modeling technique, which is usually constructed based on the image information from the computed tomography (CT) or magnetic resonance imaging (MRI) of the patient. According to statistics, when Monte Carlo particle transport simulations are performed, about 30% - 80% of the computational time is spent on geometry processing, so the MagicDose program combines the characteristics of CT/MRI image information and the advantages of the lattice structure geometry processing method, which has a better average efficiency compared to the constructive solid geometry (CSG) method. Firstly, based on the CSG method, each tissue is defined as a cubic universe according to the surface equation, and then multiple universes are arrayed and discharged to form a repetitive lattice structure, which is then combined with the database module to fill in the nuclide composition and ratio of the corresponding tissue region, so as to construct a complex dose calculation model. Fig. 4 shows the lattice mapping to the geometric model.

(2) Source module: It is very important to determine the source of BNCT irradiation in TPS because it involves a 5-dimensional (X, Y, Z, E, Ω) probability distribution that accurately describes the spatial, energy, and angular characteristics of the neutron beam. MagicDose program supports a variety of commonly used source terms, including point source of the monodirectional angular distribution, point source of the isotropic angular distribution, spatial source of the isotropic angular distribution, spatial plane source with translation and rotation, etc. It is capable of simulating neutron, photon, and neutron-photon coupled transport, and supports a variety of probability distributions (discrete, continuous, histogram, and mixed distribution) for the corresponding source parame-
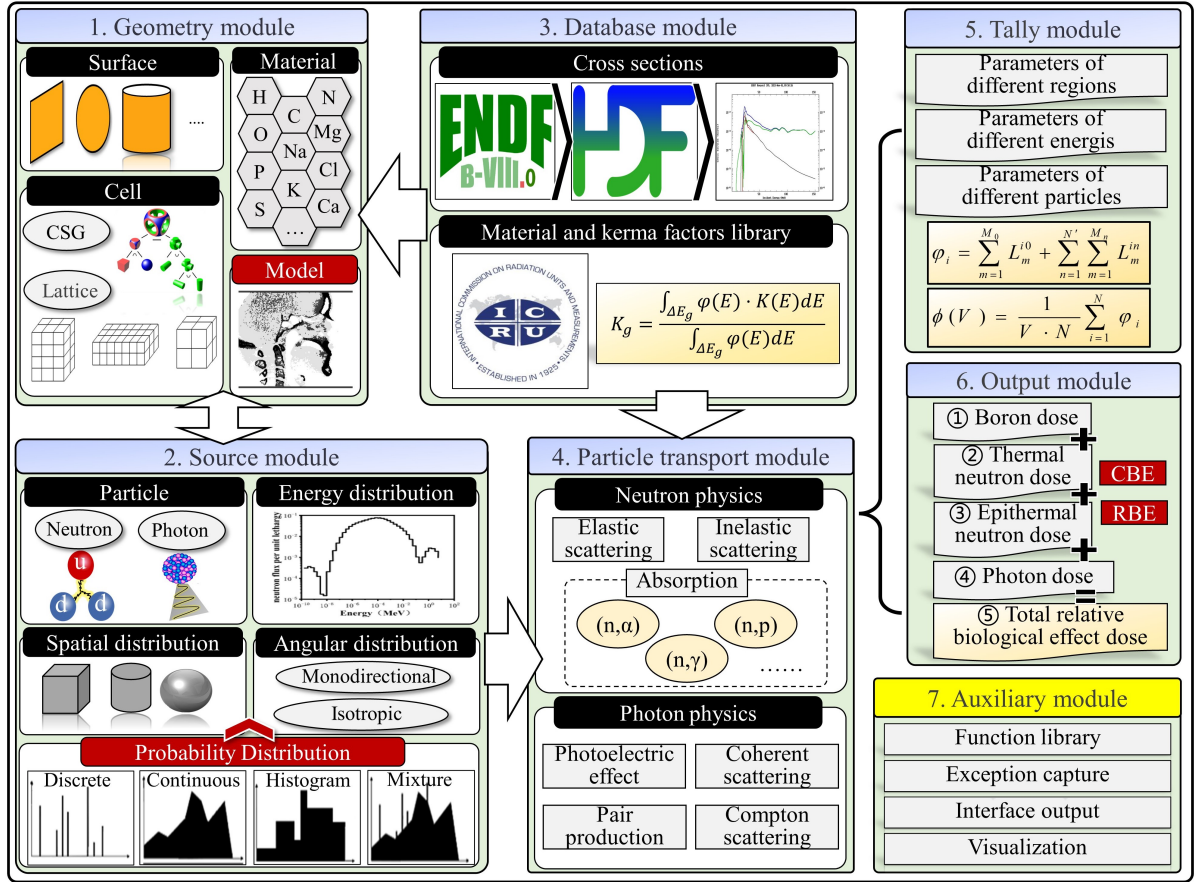
Fig. 3. Development framework of MagicDose.

ters, which provides an effective tool for simulating complex source beams for BNCT.

Fig. 5(a) shows the schematic diagram of an in-hospital neutron irradiator type I reactor (IHNI-I), which is the first prototype in the world that meets the requirements of the IAEA-specialized neutron source device BNCT [15]. The IHNI-I has a "tank-pool" structure with a rated power of 30 kW and two beam holes for thermal and epithermal neutrons [16]. MagicDose establishes equivalent planar sources at the exit of the orifice for the two beams of the IHNI-I reactor, and the spatial distributions are 0-6 cm, 6-10 cm, and 10-15 cm, which can be used for subsequent BNCT simulations. Fig. 5(b)(c) denote the energy spectral distributions of the thermal neutron beam and the energy spectral distributions of the epithermal neutron beam, respectively.

(3) Database module: In particle transport calculation, the microscopic cross-section, and the angular distribution data of nuclear reactions induced by particles of various energy segments and various nuclides are involved. Meanwhile, because a low-energy neutron contributes a lot to the dose of BNCT, when the neutron energy is reduced to a few eV, the thermal motion of the scattering target nucleus will have a strong effect on the collision, which will affect the energy of the emitted neutron and the exit angle, and eventually

lead to errors in the results. MCNP provides $S(\alpha,\beta)$ thermal scattering model for this case, which directly calls the $S(\alpha,\beta)$ thermal scattering model data from the corresponding nuclides [17]. The MagicDose program also saves the same $S(\alpha,\beta)$ thermal scattering data for the thermal neutron scattering of H in the voxel phantom material. Magic-Dose program stores the physically relevant data of each reaction cross-section in particle transport based on the ENDF/B-VIII.0 evaluation database using HDF5 data format which has the advantages of hierarchical structure and can handle large data sets [18]. The actual tissue components need to be simulated in the calculation of the BNCT dose, and according to the ICRU46 and ICRU63 reports [19, 20], a material library including 106 human tissue components (Table 2) and the corresponding Kerma factor library (Fig. 6), with functions to support the addition, modification, and editing of the related data. The Kerma factor library is built according to Eq. (1) and Eq. (2) [16].

$$K_g = \frac{\int_{\triangle E_g} \varphi(E) \cdot K(E) \, dE}{\int_{\triangle E_g} \varphi(E) \, dE} \tag{1}$$

Where K_g is the average Kerma factor of the neutron or γ-photon in group g with the unit of Gy·cm^2; $\triangle E_g$ is the width of the energy group region of group g; $\varphi(E)$ is the neutron or
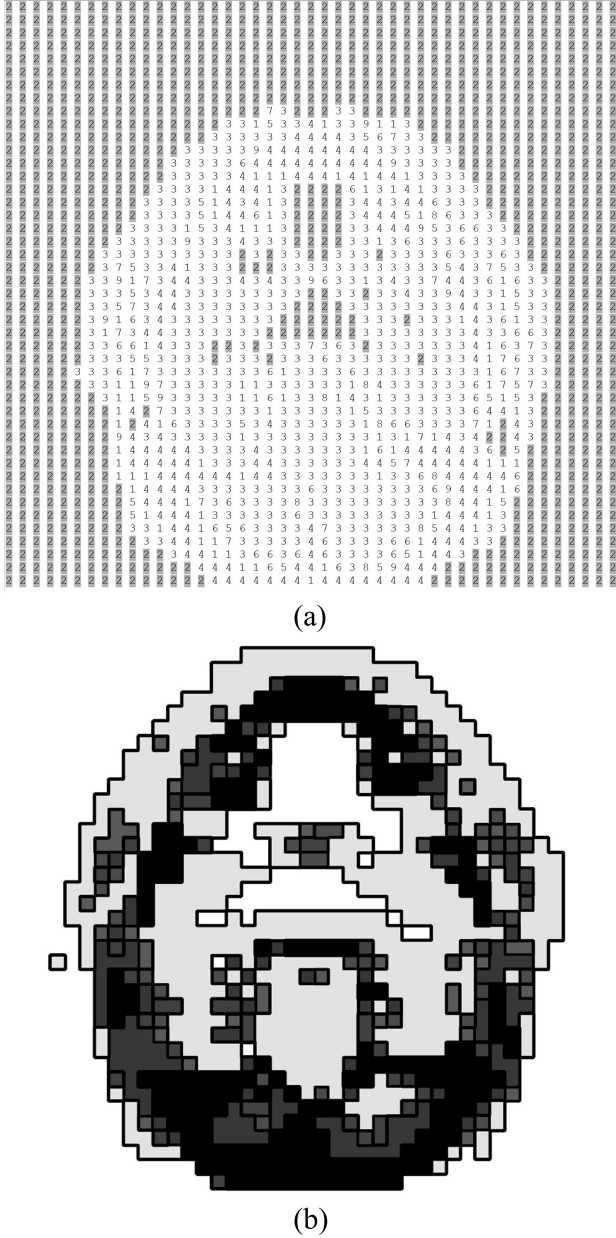
(a)

(b)

Fig. 4. **(a)** Lattice in input card; **(b)** Model.

γ-photon energy spectrum E with the unit of n/cm^2·s; $K(E)$ is the Kerma factor at energy point E with the unit of Gy·cm^2. Data from the ICRU46 report can be used directly for neutron in different tissues of the human body, but $K_\gamma(E)$ for γ-photon needs to be derived by conversion from Eq. (2).

$$K_\gamma(E) = \frac{E \cdot \mu_{en}(E)}{\rho} \qquad (2)$$

Where $\mu_{en}(E)/\rho$ is the mass-energy absorption coefficient of γ-photon in the ICRU46 report with the unit of cm^2·kg^{-1}; E is the γ-photon energy with the unit of J. The Kerma factor database of multigroup neutron and γ-photon is obtained by combining Eq. (1) and Eq. (2) with the energy spectra of the

ICRU46 report.

(4) Particle transport module: BNCT dose calculation is the neutron-photon coupled transport process, and this module deals mainly with the MagicDose program to simulate the particle production to disappearance process. For the neutron-matter interaction, it mainly involves elastic scattering, inelastic scattering, and absorption, in which the absorption contains the dose-dependent reactions of interest to the BNCT (n,α), (n,p) and (n,γ), and so on. During this process, the induced photon generated by a neutron will be stored in a particle bank to be ready for subsequent photon transport. With respect to the photon-matter interaction, the photoelectric effect, electron pair effect, coherent scattering, and compton scattering are mainly considered [21]. Fig. 7 shows the particle transport flow diagram.

(5) Tally module: After particle transport is completed, users can set different statistical parameters to invoke the tally module according to their own needs, among which the parameters include selection of the region of interest, the program supports two ways of statistics: cell statistic and virtual superposition mesh statistic, and supports setting of energy region and particle type, etc. The corresponding quantity of flux ϕ is obtained in various statistical ways, and the data of each dose component can be obtained by combining Eq. (3) and the Kerma factor library in the database module.

$$Dose(j) = \int \frac{\phi(j,E)}{V(j)} \cdot Kerma(j,E)dE \qquad (3)$$

Where $\phi(j,E)$ is the normalized flux value in n·cm/s for the j_{th} voxel mesh with energy E; $V(j)$ is the volume of the j_{th} voxel mesh, and $Kerma(j,E)$ is the neutron/photon flux dose conversion factor for the j_{th} voxel mesh with energy E. In this paper, the Kerma factor for the adult brain relative to ICRU46 given by ICRU63 in the MagicDose program database is used, but the lowest energy corresponding to the Kerma factor given in the report is 0.0253 eV, and for the dose of the BNCT, the neutron contribution to the thermal neutron dose for energy lower than 0.0253 eV is very important. Therefore, double logarithmic interpolation is adopted to extrapolate the Kerma value corresponding to less than 0.0253 eV to the data corresponding to 0.0001 eV, and the Kerma factor of the photon in this paper is obtained based on the mass-energy absorption coefficients calculated by Seltzer [22].

(6) Output module: Data counted by the tally module is transferred to the output module, through which data export of boron dose, thermal neutron dose, epithermal and fast neutron dose, and photon dose of interest in the BNCT treatment is exported. Since different types of ionizing radiation cause different biological effects in living organisms and BNCT involves mixed-field irradiation of several different radiation dose components, for BNCT treatment, it is necessary to measure the relative biological effectiveness (RBE) dose of each dose component and assess its killing effect on normal tissue and tumor. The RBE measured experimentally is used to characterize the high or low biological effect dose of thermal neutron dose, epithermal and fast neutron dose, and photon dose. To convert the local high LET radiation dose produced
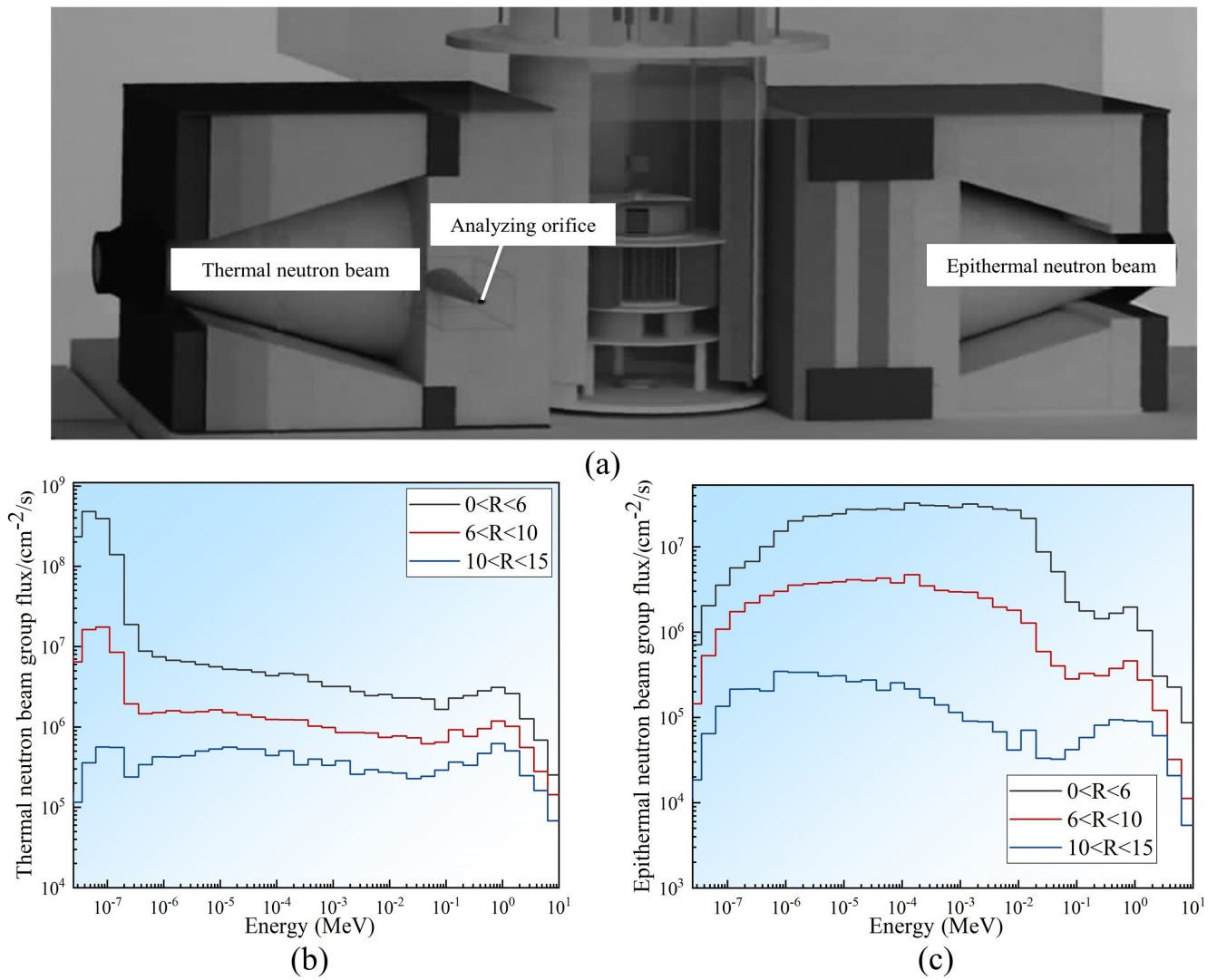
Fig. 5. **(a)** Schematic diagram of in-hospital neutron irradiator type I reactor (IHNI-I); **(b)** Thermal neutron beam energy spectral distribution; **(c)** Epithermal neutron beam energy spectral distribution.

TABLE 2. Elemental composition and density of tissues.

Tissue		Density (g/cm^3)	Elemental composition (mass percentage %)									
			H	C	N	O	Na	P	S	Cl	K	...
Brain (whole)	Fetus (14weeks)	1.02	10.90	3.30	0.70	84.20	0.20	0.20	0.00	0.30	0.20	...
	Newborn	1.03	10.80	5.50	1.10	81.60	0.20	0.30	0.10	0.20	0.20	...
	Infant (18months)	1.03	10.70	9.10	1.60	77.60	0.20	0.30	0.10	0.20	0.20	...
	Adult	1.04	10.70	14.50	2.20	71.20	0.20	0.40	0.20	0.30	0.30	...
Lung	Fetus (17-40 weeks)	1.04	10.60	7.60	1.80	79.20	0.20	0.20	0.10	0.20	0.10	...
	Adult (healthy)	0.26 (Inflated)	10.30	10.50	3.10	74.90	0.20	0.20	0.30	0.30	0.20	...
	Adult (congested)	1.04	10.50	8.30	2.30	77.90	0.20	0.10	0.20	0.30	0.20	...
	Fetus (17-40 weeks)	1.04	10.60	7.50	1.80	79.30	0.20	0.10	0.10	0.20	0.20	...
Heart	Child (2 years)	1.04	10.50	8.80	2.20	77.70	0.10	0.20	0.10	0.20	0.20	...
	Child (4-18 years)	1.04	10.50	10.40	2.50	75.70	0.10	0.20	0.10	0.20	0.30	...
	Adult (healthy)	1.05	10.40	13.90	2.90	71.80	0.10	0.20	0.20	0.20	0.30	...
	Adult (fatty)	1.04	10.30	18.20	3.10	67.40	0.10	0.20	0.20	0.20	0.30	...
	...											

307 by ^{10}B(n,α)^{7}Li into an equivalent dose, the use of a com- 308 pound biological effect (CBE) factor is required to more accu-
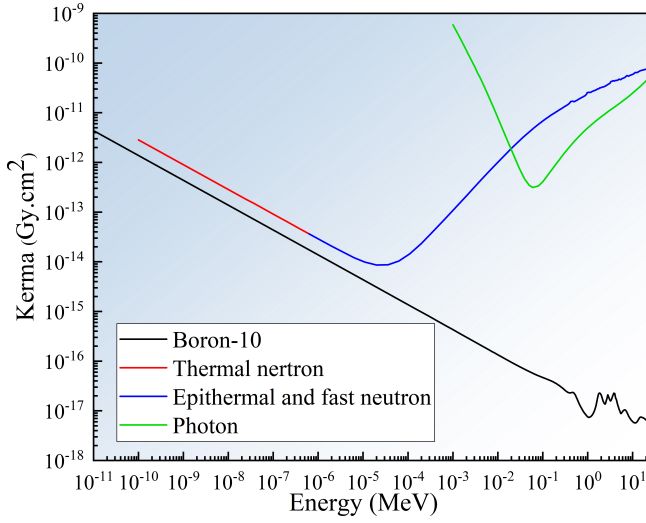
Fig. 6. Kerma value for each dose component.

rately assess its actual biological effects on biological tissues, especially tumors and normal tissues [23, 24]. Multiplying each of the above four dose components by their corresponding weighting factors yields the total relative biological effect dose H (Eq. (4)).

$$H = W_B D_B + W_\gamma D_\gamma + W_n D_n + W_P D_P \qquad (4)$$

Where W_B is the CBE factor for the boron dose; W_γ, W_n, and W_P are the RBE factors for the photon, epithermal and fast neutron, and thermal neutron dose, respectively; and D_B, D_γ, D_n, and D_P are the boron dose, the photon dose, the epithermal and fast neutron dose, and the thermal neutron dose from nitrogen capture, respectively.

(7) Auxiliary module: The auxiliary module is used to enhance the main functions, and improve program maintainability and user-friendliness, including the provision of related function libraries, such as mathematical libraries related to each mathematical probability sampling in the source sampling (Math), and file manipulation functions, etc. in order to improve code reusability. At the same time, program stability is enhanced by the exception catching mechanism (fatal error, warning), which detects and handles abnormalities during operation to prevent the whole program from crashing. The visualization tool in the auxiliary module shows the results of the output module, which presents the results of each BNCT dose field in 2D/3D form. Interface information outputs provide key information to the user, including run status, progress reports, run date, and number of threads, to facilitate user interaction with the program.

MagicDose program takes the particle transport module as the core, interconnects with the upstream geometry module, source module, and database module, and supports the downstream tally module and output module at the same time. Each module is independent of the other, and the module functions are realized by messages passing through the interface, which is conducive to the maintenance and expansion of the program.
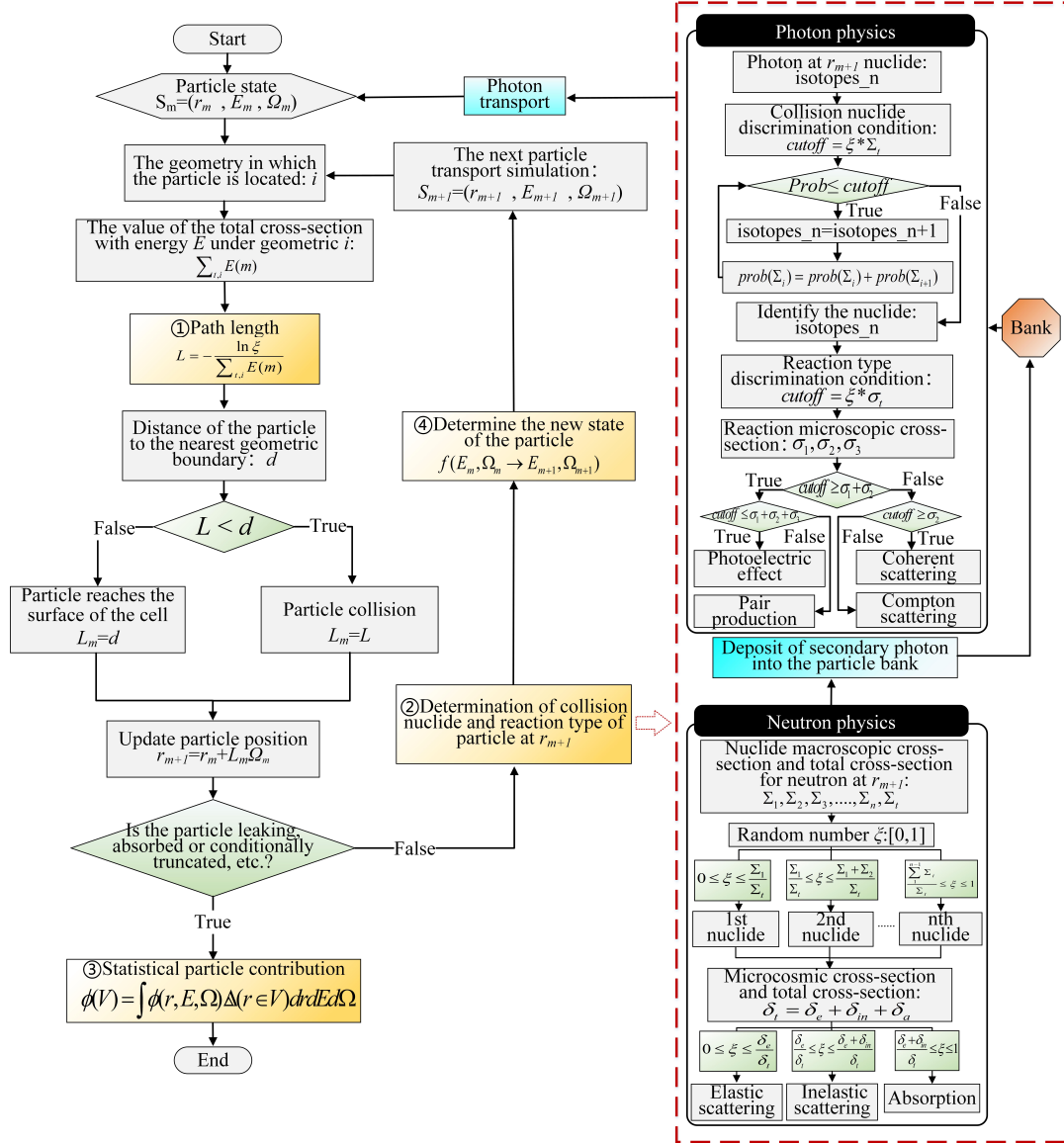
B. Calculation conditions and models

In order to fully verify the correctness and efficiency of MagicDose, three models are selected for testing. First, since the MCNP program can be used as a standard for all kinds of Monte Carlo calculations and is often used to calibrate the correctness test of other Monte Carlo programs, the results of MagicDose calculations are compared with MCNP. The two programs have selected the voxel phantom of a modified Snyder head with 16,8 mm resolution, commonly used internationally. Under the same irradiation conditions, we compare the calculated spatial neutron and photon dose rates to see if they are consistent, and we also count the computational efficiency of both; Subsequently, in order to explore the influence of voxel phantom on the calculation results under different spatial resolutions, the MCNP computational analytical model is used as the reference result. The voxel phantom of the modified Snyder head with tumor with three different spatial resolutions of 16, 8, and 1 mm are constructed using MagicDose combined with the material-located method with the central point algorithm. Through the results of depth-dose-rate curves and spatial value distribution plots, to analyze the effect of model voxel size on the results, and to statistically calculate the computational efficiency of MagicDose with different resolutions and number of threads; Finally, based on the CT head model of a patient given by DICOM data, it is initially verified whether MagicDose can be applied to the clinical case of BNCT.

All calculations in this paper are performed on an Inter(R) Core(TM) i7-10700 K CPU @ 3.8 GHz with 32 GB RAM and 16 threads, and to minimize the impact of the results from the deep penetration of the Monte Carlo program, the number of particles is set to 1×10^8 for both MagicDose and MCNP to ensure that the number of samples is adequate. In the actual BNCT treatment, some photons are produced by the accompanying neutron source, which cannot be avoided, and this paper assumes that there is no accompanying photon contamination from the neutron source and only discusses the induced photons produced by the reaction of neutrons with nuclides in the voxel.

(1) Voxel phantom of modified Snyder head with 16, 8 mm

Currently, the benchmark problem commonly adopted internationally for BNCT dose calculation is the modified Snyder head phantom, which consists of three ellipsoidal surfaces to define the boundaries of different tissues, dividing the head from inside to outside into three parts: brain tissue, skull, and scalp tissue, and the whole head is surrounded by air, which is usually called the analytical model (Fig. 8). The densities of air, scalp, skull and brain tissue are 0.001293, 1.09, 1.61 and 1.04 g/cm^3, respectively, and the corresponding elements of human tissue are obtained from the MagicDose database module, with the specific parameters shown in Table 3.

The surface analytic equations of the modified Snyder head phantom with tumor at each interface can be expressed as follows:

Boundary surface of scalp and air:

Fig. 7. Particle transport flow diagram.

$$f_1(x,y,z) = (\frac{x}{7.3})^2 + (\frac{y}{10.3})^2 + (\frac{z}{8.8})^2 = 1 \quad (5)$$

Boundary surface of skull and scalp:

$$f_2(x,y,z) = (\frac{x}{6.8})^2 + (\frac{y}{9.8})^2 + (\frac{z}{8.3})^2 = 1 \quad (6)$$

Boundary surface between brain and skull:

$$f_3(x,y,z) = (\frac{x}{6})^2 + (\frac{y}{9})^2 + (\frac{z-1}{6.5})^2 = 1 \quad (7)$$

In clinical treatment, due to the different shapes, locations, and sizes of patients' tumors, it is not possible to use analytical equations to describe the phantom, so it is common to use continuous and uniform cubic mesh to approximate the phantom structure in international clinics, which are generally called the voxel phantom. J.T. Goorley *et al* [3] construct 16,

TABLE 3. Elemental composition and density of tissues.

Elemental composition	Tissue (mass percentage %)			
	Air	Scalp	Skull	Brain
H	0.00	10.00	5.00	10.70
C	0.01	20.40	21.20	14.50
N	75.53	4.20	4.00	2.20
O	23.18	64.50	43.50	71.20
Na	0.00	0.20	0.10	0.20
Mg	0.00	0.00	0.20	0.00
P	0.00	0.10	8.10	0.40
S	0.00	0.20	0.30	0.20
Cl	0.00	0.30	0.00	0.30
K	0.00	0.10	0.00	0.30
Ca	1.28	0.00	17.60	0.00

Fig. 8. Schematic of modified Snyder head.

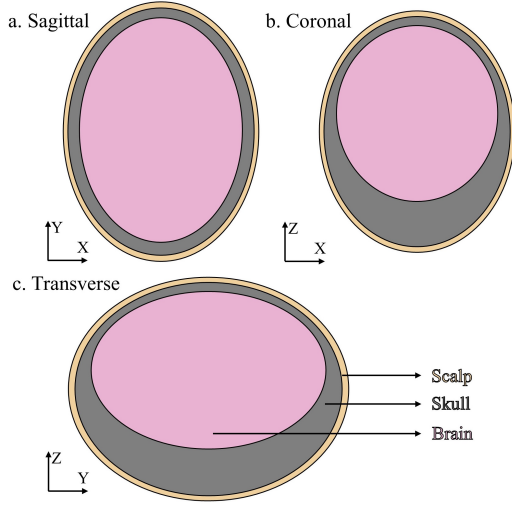432 neutron source.

Fig. 10. Energy spectra of the wide-spectrum epithermal mixed neutron beam.

412 8 mm voxel phantoms as an international benchmark problem
413 based on the modified Snyder's analytical model, which is
414 mixed with four basic materials (brain, skull, scalp, and air),
415 the volume share of each basic material in the mix is a mul-
416 tiple of 10% to produce the mixed materials and correspond-
417 ing mixing densities, and a total of 286 hybrid materials are
418 derived. Therefore, to verify the correctness of MagicDose,
419 identical 16, 8 mm voxel phantoms are constructed based on
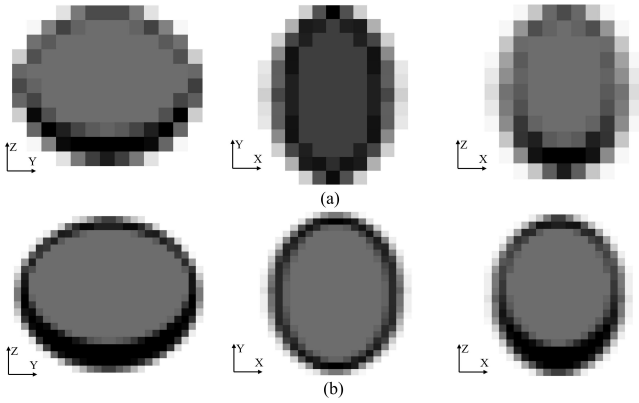420 MagicDose and MCNP respectively (Fig. 9).

Fig. 9. Voxel phantom of modified Snyder head with **(a)** 16 mm, **(b)** 8 mm.

421   For the irradiation condition, in this paper, the international
422 wide-spectrum epithermal mixed neutron beam proposed for
423 the modified Snyder head phantom is adopted, in which the
424 thermal neutron with energy less than 0.5 eV accounts for
425 10%, the epithermal neutron with energy between 0.5 eV and
426 10 keV accounts for 89%, and the fast neutron with energy
427 between 10 keV and 2 MeV accounts for 1%. Overall neutron
428 source spectra obeys the distribution according to the energy-
429 dependent probability function 1/E, uniformly distributed on
430 the disk surface with a radius of 5 cm, with a source strength
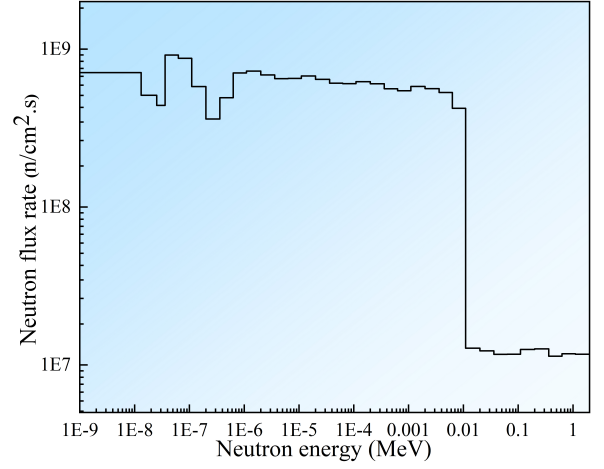431 of 10^{10} n/cm^2 ·s. Fig. 10 shows the energy spectrum of the

(2) Voxel phantom of modified Snyder head with tumor based on the material-located method with central point algorithm

436   In order to study the influence of the voxel phantom on the
437 calculation results under different spatial resolutions, as well
438 as to simulate the situation of glial tumors in the brain in the
439 clinic. In this paper, based on the model of Fig. 8, a sphere
440 with a radius of 1.5 cm is added to the brain tissue as the tu-
441 mor boundary, and the coordinate origin is at the center of the
442 entire analytical model, Fig. 11 shows the modified Snyder
443 head phantom with tumor [25, 26], in which the equation of
444 the boundary surface of the tumor and the brain is Eq. (8).

$$f_4(x, y, z) = (\frac{x}{1.5})^2 + (\frac{y}{1.5})^2 + (\frac{z - 2.8}{1.5})^2 = 1 \qquad (8)$$
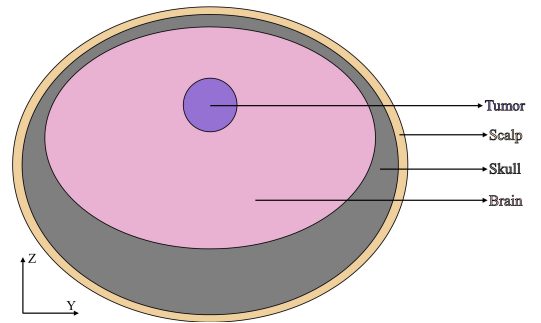

Fig. 11. Schematic transverse of modified Snyder head with tumor.

446   For the analytical model, the materials can be accurately
447 described, but the voxel phantom will be difficult to deal with
448 because the voxel mesh may be at the interface of the two sub-
449 stances, and the traditional way to deal with this is to fill by
450 obtaining the exact volume ratio of different materials inside
451 each cubic mesh (Fig. 9), which is extremely time-consuming
452 and brings some bias when the number of voxel meshes is

large. As described above, the material of the model is derived 286 from 4 materials as a hybrid material. In this paper, in order to reduce the complexity of the simulation problem, the material of the center point of the mesh is used in the phantom construction of the MagicDose, and the material density of the whole mesh is determined according to the location of the center point of each mesh, which is reduced from the original 286 kinds of material to 4 kinds of materials [27], Fig. 12 is the material-located method with the central point algorithm. In Fig. 12, (X_m, Y_m, Z_m) denotes the center point position of each voxel mesh, and $f_1(X_m, Y_m, Z_m)$, $f_2(X_m, Y_m, Z_m)$, $f_3(X_m, Y_m, Z_m)$ and $f_4(X_m, Y_m, Z_m)$ denote the boundary equations Eq. (5) - (8), respectively. When the position of the center point is substituted in the boundary equations with a value less than 1, it is "True", the mesh material is the tissue component inside the boundary equation, otherwise it is "False", the mesh material is the tissue component outside the boundary equation.

Based on the material-located method with the central point algorithm, MagicDose has constructed three voxel phantoms of the modified Snyder head with tumor with different spatial resolutions (16 mm, 8 mm, 1 mm), and the corresponding voxel mesh numbers of $M_x \times N_y \times L_z$ are 2744, 21952, and 11239424, respectively [28]. As shown in Fig. 13 the transverse view for different voxel phantoms.
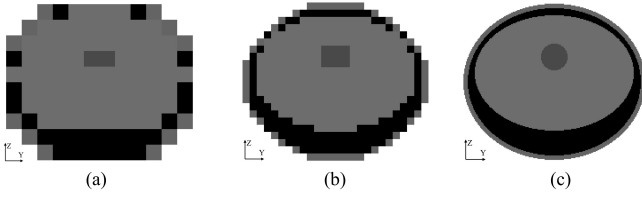

Fig. 13. Transverse view of voxel phantom of modified Snyder head with tumor at (a) 16 mm, (b) 8 mm, (c) 1 mm spatial resolution.

In this paper, MCNP is used to construct the modified Snyder head analytical model with a tumor in this part, and the results of the MCNP computation are used as the reference result, which is compared and verified with the results of MagicDose under different resolutions, and are used to explore the influence of voxel phantom on the computational results under different spatial resolutions. The tissue compositions in which the voxel phantom of the modified Snyder head with tumor and the modified Snyder head analytical model with tumor are shown in Table 3. The tissue compositions of the tumor are consistent with normal brain tissues, except for the different boron content, referring to the relevant literature [29]. According to the current clinical trials requirements, the ^{10}B content (T) of the tumor must be higher than the ^{10}B content (N) of the normal tissue by a factor of 2.5 or more (T/N > 2.5), and the calculations in this paper set the boron concentration of scalp tissue and normal tissue in the brain at 10 ppm and the boron concentration within the tumor tissue at 30 ppm, with no boron in the skull [30]. The same irradiation conditions taken by MagicDose and MCNP in this part are shown in Fig. 10. In order to make the calculation results comparable with the international BNCT dose results,

according to Eq. (4). The RBE and CBE factors are selected with reference to the values obtained from MIT and BNL in the BNCT clinical trials [31, 32], as shown in Table 4.

TABLE 4. RBE and CBE factors for tumor and healthy tissues at different dose compositions in voxel phantom of modified Snyder head with tumor.

BNCT dose components	Healthy tissue (brain, skull, scalp)	Tumor
^{10}B(n, α)^{7}Li (W$_B$-CBE)	1.35	3.8
^{14}N(n, p)^{14}C (W$_P$-RBE)	3.2	3.2
Epithermal and fast neutron (W$_n$-RBE)	3.2	3.2
Photon (W$_\gamma$-RBE)	1	1

(3) CT head model of a patient based on DICOM data

In the preliminary application, MagicDose constructs a voxel phantom based on DICOM data from a patient's head, Fig. 14 shows the coronal, transverse and sagittal comparison CT images [33]. The dimensions of the phantom in the X, Y and Z directions are 18, 18 and 16.5 cm, respectively, and the size of the constructed voxel is $0.1 \times 0.1 \times 0.1$ cm^3. The equivalent source of the epithermal neutron beam plane of the IHNI-I reactor using the MagicDose source module is used for the irradiation condition (Fig. **??**, and the irradiation direction is the vertical back of the head.
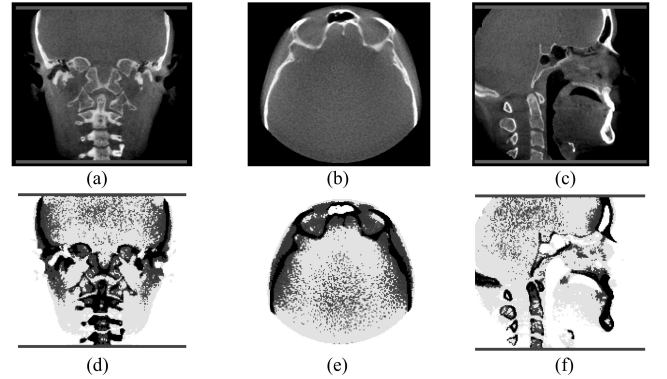

Fig. 14. (a) Coronal, (b) Transverse, and (c) Sagittal of CT images; (d) Coronal, (e) Transverse, and (f) Sagittal of MagicDose constructed model.

III. RESULT AND DISCUSSION

A. Correctness testing of MagicDose

Fig. 15 shows the comparison plots of thermal neutron dose rate, epithermal and fast neutron dose rate, and induced photon dose rate values for all voxels in the voxel phantom of the modified Snyder head at 16 mm and 8 mm spatial resolutions for MagicDose and MCNP. With MCNP as reference result [3], the slope ratio method is used in this article to distinguish how close the dose rate results calculated by MagicDose are to the MCNP results. For any voxel n in the model,
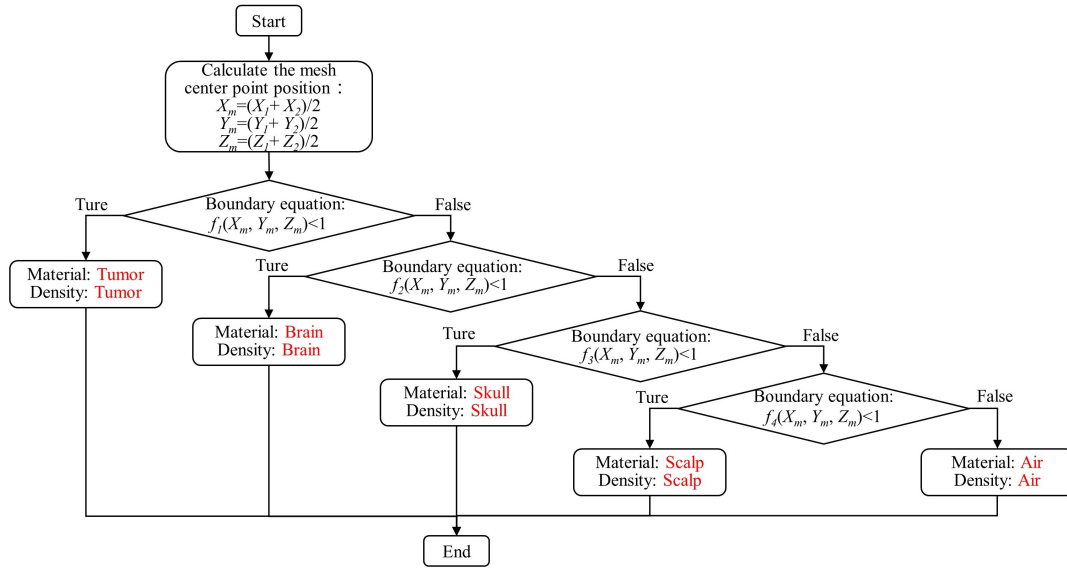
Fig. 12. The material-located method with central point algorithm.

the dose rate result of MCNP is taken as the horizontal co-ordinate value X_n, and the dose rate result of MagicDose is the vertical coordinate value Y_n, and the points (X_n, Y_n) are labeled sequentially on the coordinate system, and it is observed that all the images formed by scattering the points are scattered near the straight line equation of $y=x$. Since the number of model voxels with 16 mm spatial resolution is less compared to that of 8 mm model voxels, it can be seen from Fig. 15 that there are fewer coordinate points in 16 mm than in 8 mm, but the points (X_n, Y_n) formed by MagicDose and MCNP are all concentrated near $y=x$, and meanwhile, the local zoomed-in graphs of the respective dose rates show that the deviation of the dose rate results from $y=x$ is smaller, indicating that the results calculated by MagicDose and MCNP are in good agreement, which verifies the correctness of MagicDose.

In the calculation of the model, both MagicDose and MCNP are performed under the same conditions, as can be seen in Table 5, at a spatial resolution of 16 mm, the calculation times for MCNP and MagicDose are 1373 s and 944 s, respectively, and at a spatial resolution of 8 mm, the calculation times for MCNP and MagicDose are 2042 s and 1457 s. The numerical results demonstrate that MagicDose outperforms MCNP in terms of computational efficiency while ensuring the accuracy of the BNCT calculations.

TABLE 5. Time comparison of different computational programs based on 16, 8mm voxel phantoms.

Resolution size	Time for different calculation programs (s)	
	MCNP	MagicDose
16 mm	1373	944
8 mm	2042	1457

B. Exploration of MagicDose at different spatial resolutions

The result of each dose rate of the modified Snyder head analytical model with tumor simulated by MCNP calculation is used as the reference result in this part. In the comparative validation calculations, using the parameter setup described above (including material and source terms, etc.) as well as the nuclear cross-section database, MagicDose is used to construct voxel phantoms with three different spatial resolutions of voxel sizes of 16, 8, and 1 mm, and to compare the variability in the results of the phantom-depth correlation dose-rate curves along the Z-axis computed by the two Monte Carlo particle transport programs. At the same time, the relevant spatial dose rates of the head phantom at different voxel resolutions are statistically calculated to explore the effect of the voxel size of the voxel phantom on the results and to provide reference opinions for the optimization of the voxel phantom design for clinical treatment.

Fig. 16 - Fig. 18 show the boron dose rate, thermal neutron dose rate, epithermal and fast neutron dose rate, induced photon dose rate, and the total relative biological effect dose rate and relative deviation with depth, as well as spatial dose rate distributions at different voxel resolutions, respectively. The relative deviation is the percentage of deviation obtained by comparing the MagicDose voxel phantom results with the MCNP analytical model results as the reference result, and the ICRU24 report suggests that the relative deviation between actual treatment and the planned dose of BNCT should not exceed 5%, otherwise there will be a risk of tumor recurrence and an increase in radiological complications in normal tissues [34, 35].

As seen in Fig. 16(a), the boron dose rate calculated by MagicDose at different resolutions of the voxel is compared with the reference result, which is consistent with the results at 1 mm, but the variability of the results is more obvious with
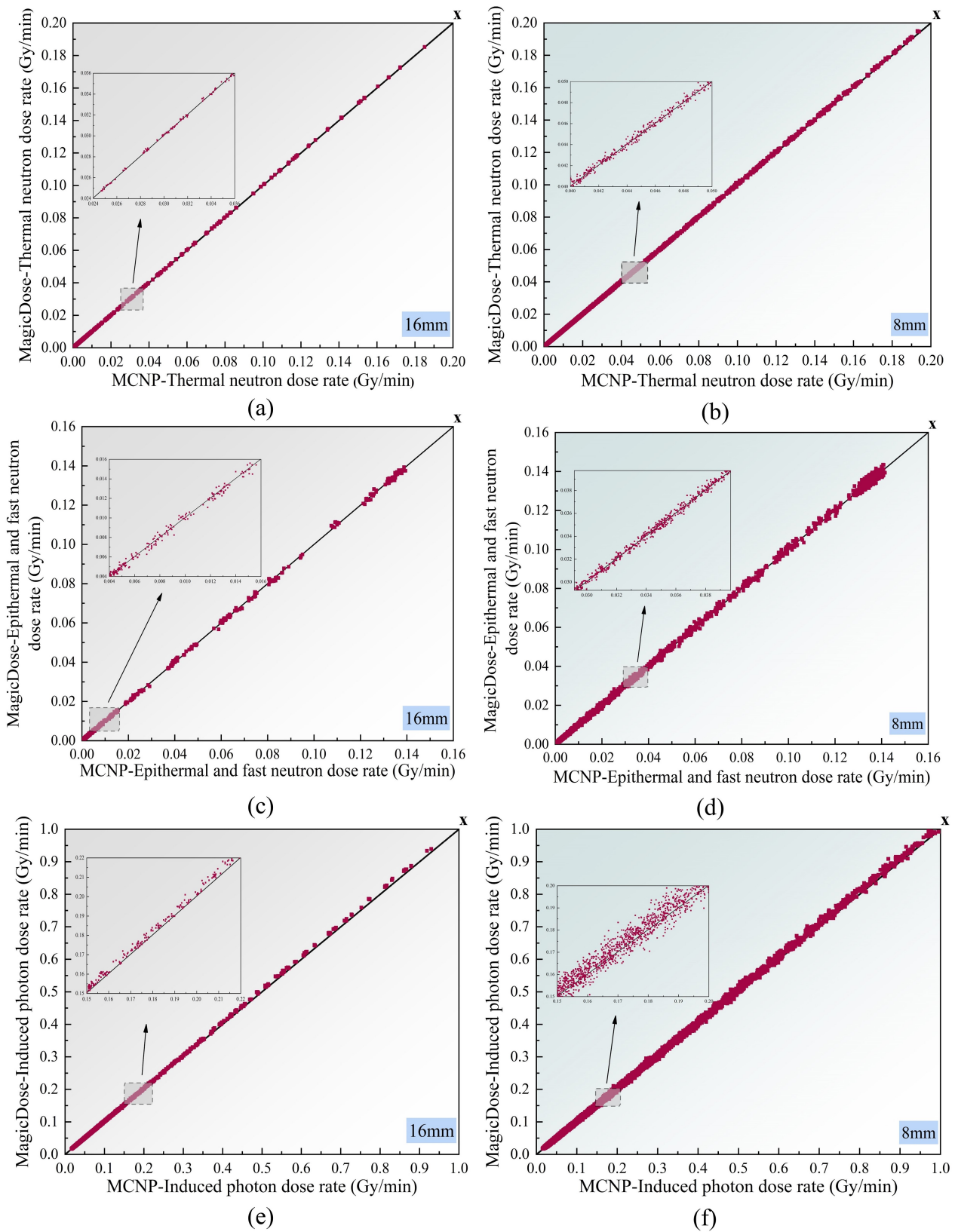
Fig. 15. **(a)(b)** Thermal neutron dose rate based on voxel phantom of modified Snyder head; **(c)(d)** Epithermal and fast neutron dose rate based on voxel phantom of modified Snyder head; **(e)(f)** Induced photon dose rate based on voxel phantom of modified Snyder head.

583 the increase in the resolution of the voxel. From Fig. 16(b), 584 it can be seen that the relative deviations of 1 mm are kept

within $\pm5\%$ of the clinical allowable for BNCT, while 8 mm and 16 mm have greater relative deviations between depths of 0.5-1.5 cm, 5.4-8.2 cm and 14.2-18.2 cm. Combining the phantom of Fig. 13 and the spatial dose rate distribution calculated by Fig. 16(c) - Fig. 16(e), the reason for the large relative deviations is that the depth of 0.5-1.5 cm, 14.2-18.2 cm is skull, and 5.4-8.2 cm is the tumor, and the phantoms of 8 mm and 16 mm don't have a high resolution of the tissues at these two places, which ultimately leads to inaccurate results of the dose rate calculation. Fig. 16(c) - Fig. 16(e) highlights that the results calculated from the voxel phantom in high resolution are more accurate, and based on the spatial dose rate values, it can be clearly judged that the skull of the head does not produce the boron dose rate because it does not contain boron. In the tumor region, the boron content is higher, resulting in a significant increase in the boron dose rate, which helps to locate the tumor more accurately in the clinic.

From Fig. 16(f) - Fig. 16(j) and Fig. 17(f) - Fig. 17(j), the thermal dose rate and the induced photon dose rate results of 1 mm and 8 mm are consistent with the reference result, and the relative deviations are kept within $\pm5\%$, but the calculated results are biased due to the large resolution of the 16 mm voxel. Meanwhile, the distribution curves of the thermal dose rate and induced photon dose rate have the same trend, and this is due to the fact that the induced photon comes from the neutron capture reaction and the γ-ray generated by the capture reaction between thermal neutron and H-atom in the body, and the photon is generated in place of the higher neutron dose, and the greatest damage is produced in the superficial tissues of the head.

It can be seen from Fig. 17(a)(c)(d)(e) that because 89% of the proportion of neutron source radiation is epithermal neutron, neutron slowing down to thermal neutron occurs at the beginning, and the dose rate gradually decreases as the depth deepens. From Fig. 17(b), it is understood that when the depth is less than 12 cm, the relative deviations of both 1 mm and 8 mm are basically kept within 5%; when the depth is greater than 12 cm, it will cause the problem of deep penetration, at which time the Monte Carlo program calculates the number of particles arriving at the depth to be less, resulting in the statistical results of the relative deviation to be larger.

Finally, the dose rates from Fig. 16 to Fig. 17 are combined according to the corresponding factors of CBE or RBE to obtain the total dose rate of the relative biological effect, as shown in Fig. 18. As shown in Fig. 18(a)(b), the total dose rate at 1 mm is consistent with the results of the reference result, and the relative deviations are kept within 5%, while the discrepancy of the results at 8 mm and 16 mm are due to the boron dose as the main dose component, and the effect of the resolution of the voxel phantom on the boron dose, which ultimately leads to the deviation of the total dose rate. Overall, Fig. 16 to Fig. 18 show that the dose rates and relative deviations of the high-resolution voxel phantoms calculated from MagicDose are consistent with the reference result and remain within $\pm5\%$, indicating that as the size of the constructed voxel mesh gets smaller, the better it converges to the analytical model, the better the computed results match, highlighting the effect of the voxel size of the voxel phantoms on the results

Since the boron concentration of BNCT will change rapidly with the body's metabolism after boron injection, this will lead to a high requirement of BNCT in terms of the speed of dose calculation, which requires that the dose calculation can be completed in a very short period of time (<3600 s), and the number of voxels also affects the efficiency of the calculation. Therefore, in order to verify the computational efficiency of MgaicDose, simulations are performed using 1, 4, 8, and 16 threads for the voxel phantom of modified Snyder head with tumor at 16, 8, and 1 mm, respectively, to test the computational efficiency of the program at different spatial resolutions and with different numbers of threads. Fig. 19 shows the comparison of computation time (s) for different mesh scales and different numbers of thread 3D histograms, from which it can be seen that under the same computational conditions, the smaller the voxel size, the longer the simulation computation time, but with the increase of the number of parallel threads, the time used for the simulation is getting shorter and shorter, with more and more obvious acceleration effects.
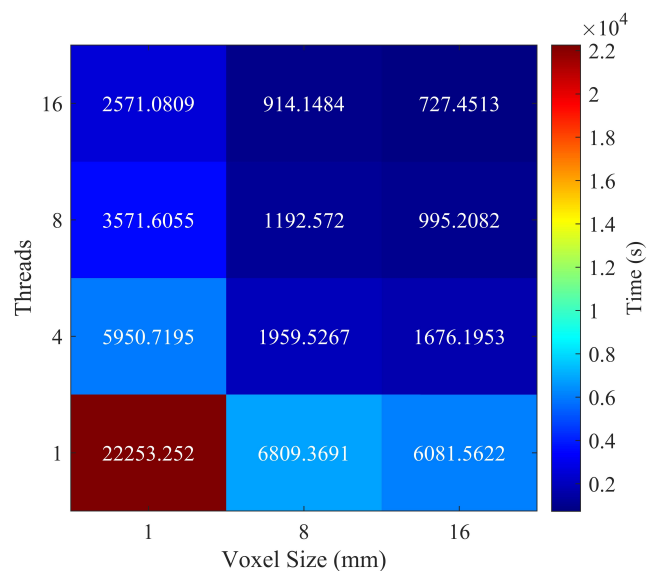

Fig. 19. Comparison of computation time (s) for different mesh scales and different number of threads 3D histograms.

C. Initial application of MagicDose based on DICOM data

From the above, it can be seen that MagicDose has constructed a voxel phantom of a head using DICOM data, and Fig. 14 shows that the schematic diagrams of MagicDose in the coronal, transverse and sagittal planes are consistent with the CT images of the corresponding locations. Fig. 20 shows the boron dose rate, thermal neutron dose rate, epithermal and fast neutron dose rate, induced photon dose rate, and the total relative biological effect dose rate obtained by combining with Table 4 for MagicDose irradiated with the epithermal neutron beam of the IHNI-I reactor. The spatial distribution
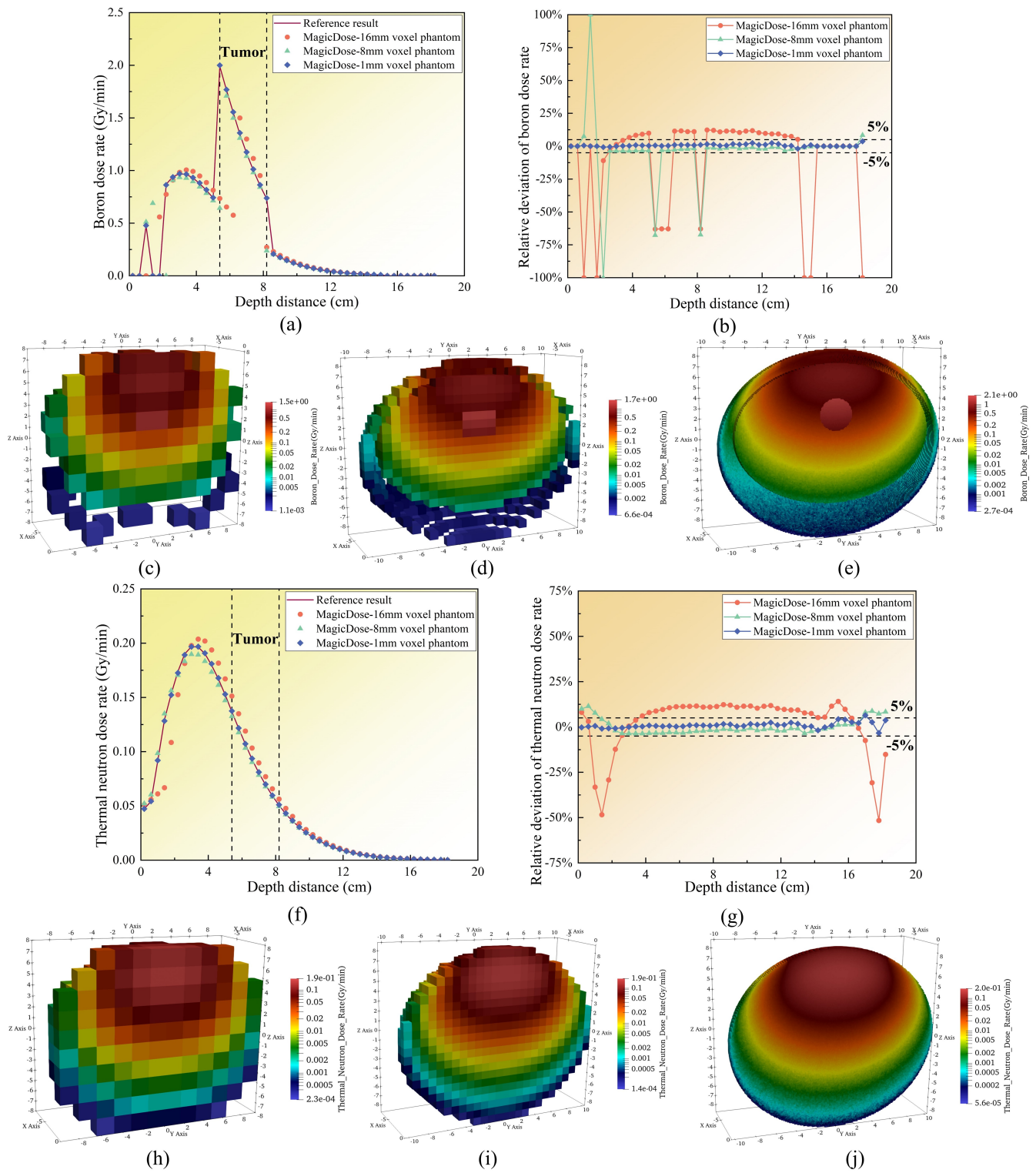
Fig. 16. **(a)(b)** Boron dose rate and relative deviation vs. depth; **(c)(d)(e)** Boron dose rate at 16 mm, 8 mm and 1 mm; **(f)(g)** Thermal neutron dose rate and relative deviation vs. depth; **(h)(i)(j)** Thermal neutron dose rate at 16 mm, 8 mm and 1 mm.

of boron dose rate and thermal neutron dose rate are similar from Fig. 20(a) and Fig. 20(b), which is due to the fact that both doses are related to thermal neutrons, and the value of boron dose rate is significantly higher than the contribution of the rest of the dose rates; the epithermal neutron dose rate presented in Fig. 20(c) is mainly located in the shallower re-
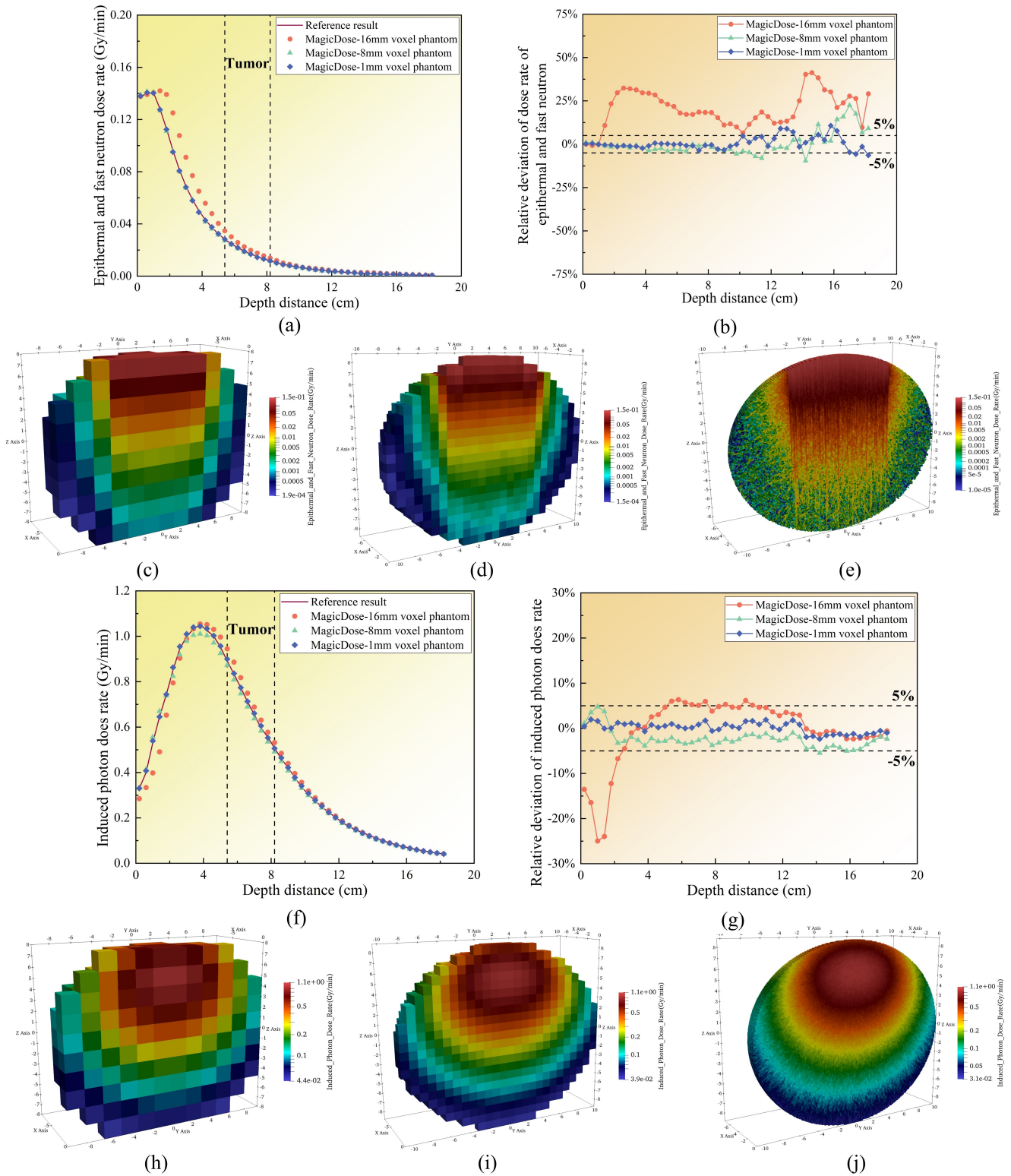
Fig. 17. **(a)(b)** Epithermal and fast neutron dose rate and relative deviation vs. depth; **(c)(d)(e)** Epithermal and fast neutron dose rate at 16 mm, 8 mm and 1 mm; **(f)(g)** Induced photon dose rate and relative deviation vs. depth; **(h)(i)(j)** Induced photon dose rate at 16 mm, 8 mm and 1 mm.

681 gion of the posterior cerebral epidermis; From Fig. 20(d), it 682 is understood that the induced photon dose rate is distributed 683 throughout the space and presents the complete human head 684 profile; combining the CBE and RBE factors, the total relative
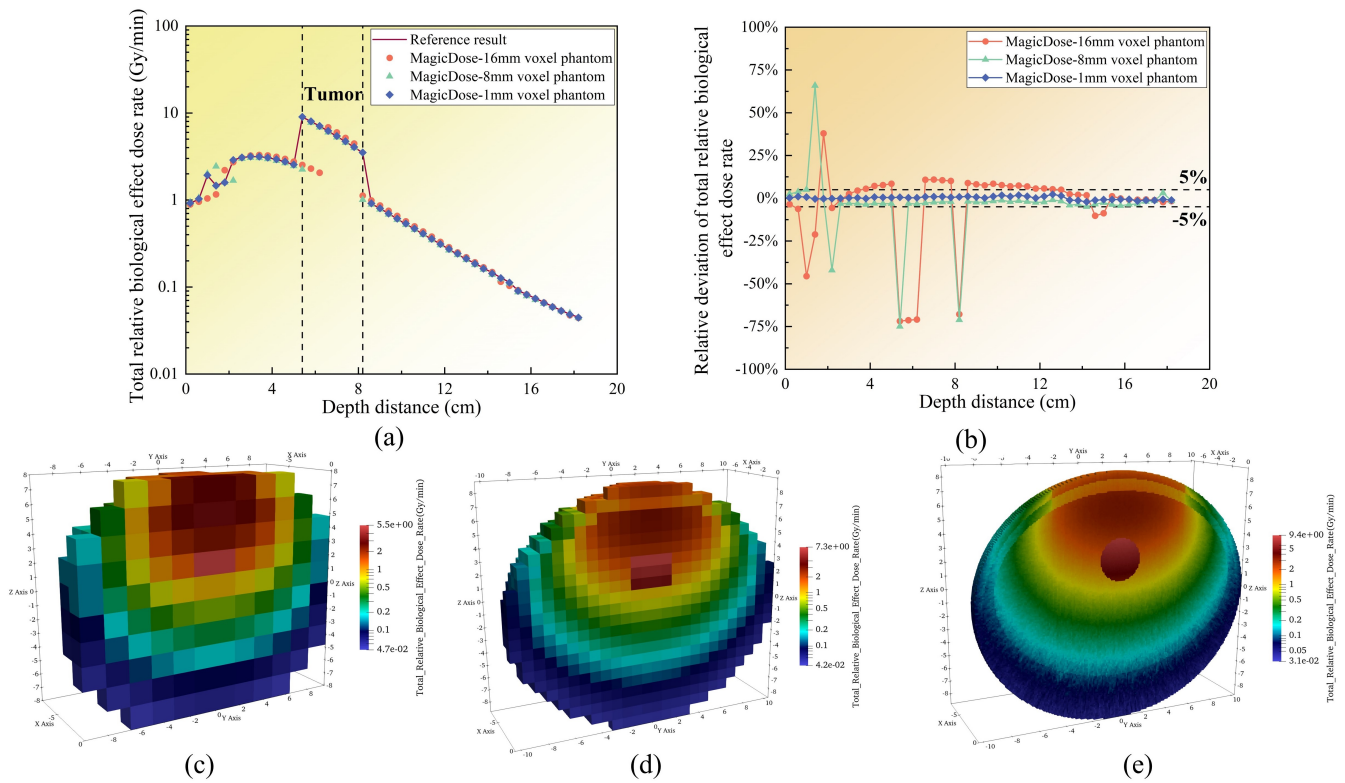
Fig. 18. **(a)(b)** Total relative biological effect dose rate and relative deviation vs. depth; **(c)(d)(e)** Total relative biological effect dose rate at 16 mm, 8 mm and 1 mm.

bioeffect dose rate of Fig. 20(e) is obtained, and the highest dose region occurs in the irradiated region of the back of the head.

IV. CONCLUSION

In order to further develop the TPS-dedicated dose calculation program for BNCT, this paper has developed the BNCT Monte Carlo Dose Calculation Program MagicDose based on the Monte Carlo Particle Transport method, which has a small program size, a high degree of specialization, and a high degree of autonomy compared to MCNP. Magic-Dose involves seven functional modules, namely, geometry, source, database, particle transport, tally, output, and auxiliary. With particle transport as the core, connected upward with the geometry, source and database modules, and supported downward by the tally and output modules, the program adopts a modular design, so that each functional module can be developed and maintained independently, facilitating secondary development of the BNCT's subsequent needs. To test the correctness of MagicDose, two international benchmark voxel phantoms, i.e., the voxel phantom of modified Snyder head with 16, 8 mm, are firstly selected in this paper, and the neutron and photon dose rates computed by Magic-Dose and MCNP are compared with each other, which are used to validate the correctness of the program; Subsequently,

based on the material-located method with central point algorithm, three different spatial resolutions (16, 8, 1mm) of voxel phantom of modified Snyder head with tumor are constructed using MagicDose, and the depth-dose rate curve results and spatial value distribution plots are used to explore the influence of the voxel phantoms on the calculation results under different spatial resolutions; Finally, based on the CT head model of a patient given by DICOM data, Magic-Dose is used to construct a voxel phantom with a voxel size of $0.1 \times 0.1 \times 0.1$ cm^3, and the corresponding dose rate values are calculated and obtained, demonstrating the application of the program in clinical cases of BNCT. Based on the three models, the following conclusions are specifically obtained:

(1) Voxel phantom of modified Snyder head at 16 mm and 8 mm spatial resolution, using the MCNP calculation results as the reference result, the slope ratio method is used to derive that the thermal neutron dose rate, epithermal and fast neutron dose rate, and induced photon dose rate calculated by Magic-Dose are all concentrated near $y=x$. This shows that there is a good consistency between the results of the MagicDose and the MCNP calculations, and verifies the correctness of Mag-icDose. Meanwhile, the numerical results demonstrate that the efficiency of MagicDose calculation is also better than that of MCNP.

(2) The boron dose rate, the thermal neutron dose rate, epithermal and fast neutron dose rate, induced photon dose rate, and the total relative biological effect dose rate calculated
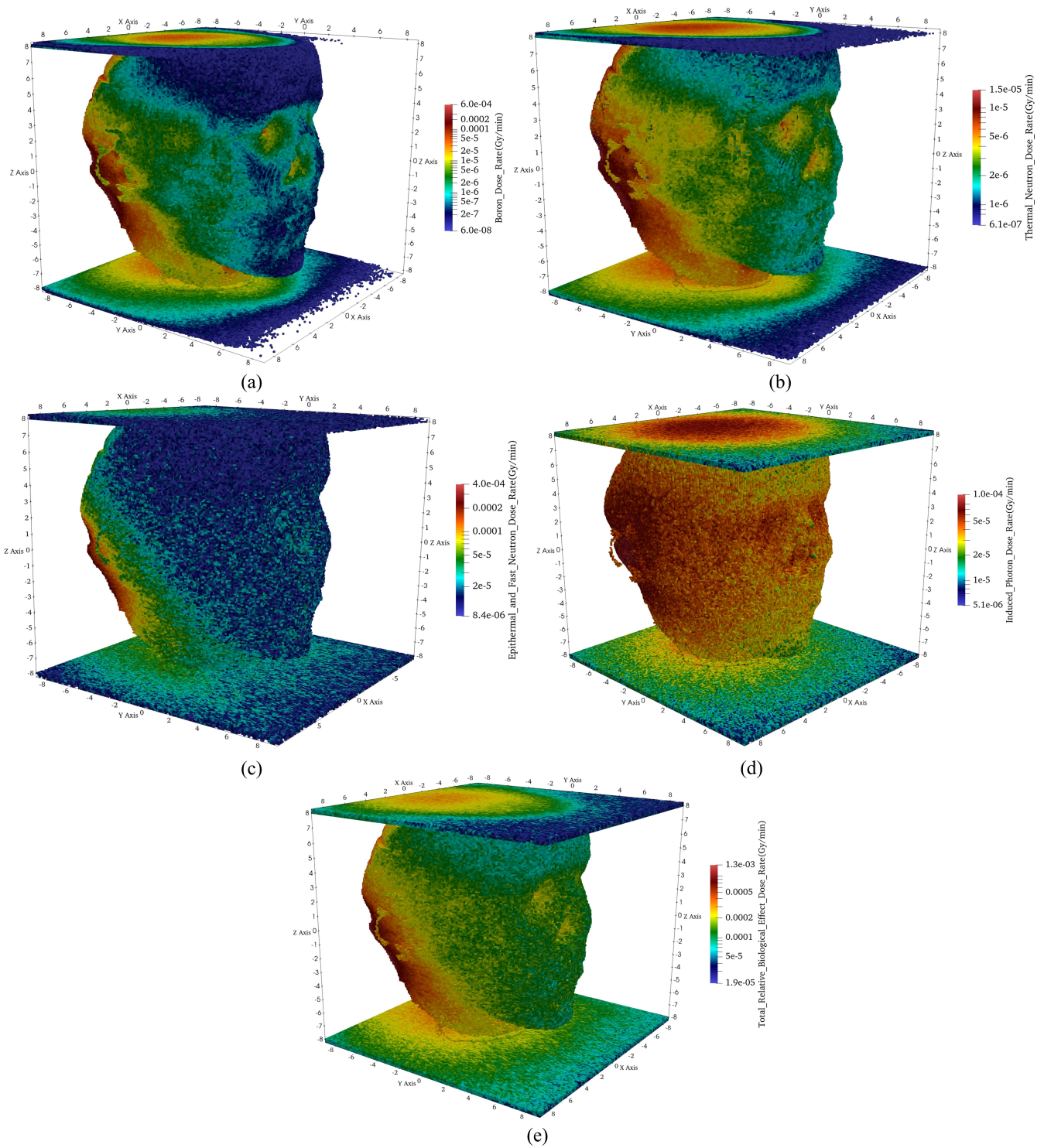
Fig. 20. **(a)** Boron dose rate distribution based on head CT; **(b)** Thermal neutron dose rate distribution based on head CT; **(c)** Epithermal and fast neutron dose rate distribution based on head CT; **(d)** Induced photon dose rate distribution based on head CT; **(e)** Total relative biological effect dose rate based on head CT.

for the voxel phantom at high spatial resolution are consistent with the reference result of the MCNP calculations, with a relative deviation less than 5%, which satisfy the requirements of clinical treatment on the accuracy of calculation. Meanwhile, the results show that the variability of the results is smaller with increasing spatial resolution, which provided reference opinions for optimizing the design of voxel phantoms in clinical treatment. In tests at different spatial resolu-

tions and with different numbers of threads, it is concluded that the smaller the size of the voxel constructed by Magic-Dose, the longer the simulation computation time, but with increasing number of parallel threads, the time used for the simulation becomes shorter and shorter, and the acceleration effect becomes more and more obvious.

(3) MagicDose is able to construct appropriate voxel phantom based on DICOM data, and the results of the calculations provide a preliminary validation of the use of the program in clinical cases, in particular, the ability to develop high-resolution CT-based phantom dosimetry calculations.

Since there is still much room for optimization of the MagicDose program, a set of four-dimensional dynamic Monte Carlo program for BNCT pharmacokinetics will be developed in the future in conjunction with the exploration of time-dependent Monte Carlo particle transport methods for more efficient and accurate dose calculations.

V.   ACKNOWLEDGMENT

VI.   CREDIT AUTHORSHIP CONTRIBUTION STATEMENT

Aikou Sun: Methodology, Software, Validation, Investigation, Visualization, Formal analysis, Writing – original draft, Writing – review & editing. **Zhenping Chen**: Conceptualization, Methodology, Validation, Supervision, Funding acquisition, Writing – review & editing. **Kekun Gao**: Methodology, Investigation, Visualization, Writing – review & editing. **Lin Zhu**: Methodology, Investigation, Visualization, Writing – review & editing. **Chengwei Liu**: Methodology, Investigation, Visualization, Writing – review & editing. **Zhiqiang Wu**: Methodology, Investigation, Visualization, Writing – review & editing. **Chao Yang**: Methodology, Investigation, Visualization, Writing – review & editing. **Tong Liu**: Methodology, Investigation, Writing – review & editing. **Song Wang**: Methodology, Investigation, Writing – review & editing. **Zizhu Zhang**: Methodology, Investigation, Writing – review & editing. **Yizheng Chong**: Methodology, Investigation, Writing – review & editing. **Tao Yu**: Supervision, Writing – review & editing, Funding acquisition.

[1] B.F. Han, R.S. Zheng, H.M. Zeng et al., Cancer Incidence and Mortality in China, 2022. J Natl Cancer Cent. vol. **4**, no. 1, pp. 47-53 (2024). doi: 10.1016/j.jncc.2024.01.006

[2] INTERNATIONAL ATOMIC ENERGY AGENCY, *Advances in Boron Neutron Capture Therapy.* (Non-serial Publications, IAEA, Vienna, 2023).

[3] J.T. Goorley, W.S. Kiger Iii, R.G. Zamenhof, Reference dosimetry calculations for neutron capture therapy with comparison of analytical and voxel models. Med Phys. **29(2)**: 145-156 (2002). doi: 10.1118/1.1428758

[4] S. J. González, *NCTPlan, the New PC Version of MacNCT-Plan: Improvements and Verification of a BNCT Treatment Planning System.* (10th International Congress on Neutron Capture Therapy for Cancer, Essen, Germany, 2002).

[5] T. Seppaelae, L. Kankaanranta, H. Joensuu et al., BNCT Rtpe and SERA dose Planning Programs: Phantom and Patient Studies. (2000).

[6] N. Cerullo, G.G. Daquino, L. Muzi, An overview on the developments and improvements of a treatment planning system for BNCT. IEEE Trans Nucl Sci. **53(3)**: 1333-1338 (2006). doi:10.1109/TNS.2006.872501

[7] H. Kumada, K. Yamamoto, A. Matsumura et al., Verification of the Computational Dosimetry System in JAERI (JCDS) for Boron Neutron Capture Therapy. Phys Med Biol. **49(15)**: 3353 (2004). doi:10.1088/0031-9155/49/15/003

[8] H. Kumada, K. Takada, T. Aihara et al., Verification for dose Estimation Performance of a Monte-Carlo based Treatment Planning System in University of Tsukuba. Appl Radiat Isot. **166** (2020). doi:10.1016/j.apradiso.2020.109222

[9] N. Hu, H. Tanaka, K. Ryo et al., Evaluation of a treatment planning system developed for clinical boron neutron capture therapy and validation against an independent Monte Carlo dose calculation system. Radiat Oncol. **16**, 243 (2021). doi:10.1186/s13014-021-01968-2

[10] W.B. Zhong, J. Chen, Y.C. Teng et al., Introduction to the Monte Carlo dose engine COMPASS for BNCT. Sci Rep. **13(1)** (2023). doi:10.1038/s41598-023-38648-y

[11] T. Lin, Y.H. Liu, Development and verification of THORplan—A BNCT treatment planning system for THOR. Appl Radiat Isot. **69(12)**, 1878-1881 (2011). doi:10.1016/j.apradiso.2011.03.025

[12] L. Deng, G. Li, T. Ye et al., MCDB Monte Carlo code with fast track technique and mesh tally matrix for BNCT. J Nucl Sci Technol. **44(12)**: 1518-1525 (2007). doi:10.1080/18811248.2007.9711401

[13] Z.T. Wang, Q. Zheng, B. Wang et al., Recent Research Progress of BNCT Treatment Planning System. Nucl. Eng. Technol. Accessed October 31, (2024). doi:10.1016/j.net.2024.10.026

[14] *Neutron capture therapy: principles and applications.* (Springer Science & Business Media, 2012).

[15] Y. Zhu, X. Jiang, L. Chen et al., Study on quality parameters of neutron beams in IHNI-I reactor ducts. Progress report on nuclear science and technology in China (Vol. 4). Proceedings of academic annual meeting of China Nuclear Society in 2015, No. 7–Nuclear Physics sub-volume. 2016. (**in Chinese**)

[16] M. Amini, S.M. Zamzamian, A.H. Fadaei et al., An investigation on the improvement of neutron radiography system of the Tehran research reactor by using MCNPX simulations. Nucl. Eng. Technol. **53(10)**, 3413-3420 (2021).

doi:10.1016/j.net.2021.04.014

[17] C.D. Werner. *MCNP Users Manual-Code Version 6.2 Los Alamos National Laboratory Report LA-UR-17-29981*. Tech. rep, SS (2017).

[18] P.K. Romano, N.E. Horelik, B.R. Herman et al., OpenMC: A state-of-the-art Monte Carlo code for research and development. Ann Nucl Energy. **82**, 90-97 (2015). doi:10.1016/j.anucene.2014.07.048

[19] International Commission on Radiation and Measurements ICRU. *Photon, electron, proton and neutron interaction data for body tissues*. ICRU, (1992).

[20] International Commission on Radiation Units. *Nuclear data for neutron and proton radiotherapy and for radiation protection*. Vol. 63. International Commission on Radiation, (2000).

[21] C. Lee, H. Lee, Development of a dose estimation code for BNCT with GPU accelerated Monte Carlo and collapsed cone Convolution method. Nucl. Eng. Technol. **54(5)**, 1769-1780 (2022).doi:10.1016/j.net.2021.11.010

[22] S.M. Seltzer, Calculation of photon mass energy-transfer and mass energy-absorption coefficients.Radiat Res. **136(2)**: 147-170 (1993). doi:10.2307/3578607

[23] S. Ishiyama, Deterministic Parsing Model of the Compound Biological Effectiveness (CBE) Factor for Intracellular 10 Boron Distribution in Boron Neutron Capture Therapy. J. Cancer Ther. **5(14)**: 1388 (2014). doi:10.4236/jct.2014.514140

[24] Z. Zhang, Y. Chong, Y. Liu et al., A Review of Planned, Ongoing Clinical Studies and Recent Development of BNCT in Mainland of China. Cancers. **15(16)**, 4060 (2022).doi:10.3390/cancers15164060

[25] J.R. Albritton, *Computational aspects of treatment planning for neutron capture therapy*. (Massachusetts Institute of Technology, 2009).

[26] Y.N. Zhu, Z.K. Lin, H.Y. Yu et al., Conceptional design of an adjustable moderator for BNCT based on a neutron source of 2.8 áMeV proton bombarding with Li target. Nucl. Eng. Technol. (2024). doi:10.1016/j.net.2023.12.038

[27] G. Li, Research on Monte Carlo simulation method and software development of BNCT. (CHINA ACADEMY OF ENGINEERING PHYSICS, 2005). (**in Chinese**)

[28] M. Golshanian, A.A. Rajabi, Y. Kasesaz, Evaluation of the medical staff effective dose during boron neutron capture therapy using two high resolution voxel-based whole body phantoms. Nucl. Eng. Technol. **49(7)**, 1505-1512 (2017). doi:10.1016/j.net.2017.06.011

[29] H. Yu, C. Zheng, L. Sun, Boron Neutron Capture Therapy Dose Calculation for Tumor Modified Snyder Head Phantom Using MCNP. Atom. Energy Sci. Technol. **44(1)**: 89 (2010). (**in Chinese**)

[30] M. Marashi, Analysis of absorbed dose distribution in head phantom in boron neutron capture therapy. Nuclear Instruments and Methods in Physics Research Section A: Accelerators, Spectrometers, Detectors and Associated Equipment, **440(2)**, 446-452 (2000). doi:10.1016/S0168-9002(99)00827-X

[31] C.L. Lee, L. Zhou, R.J. Kudchadker et al., A Monte Carlo dosimetry-based evaluation of the reaction near threshold for accelerator boron neutron capture therapy. Med. Phys. **27(1)**, 192-202 (1999). doi:10.1118/1.598884

[32] R. Zamenhof, E. Redmond II, G. Solares et al., Monte Carlo-based treatment planning for boron neutron capture therapy using custom designed models automatically generated from CT data. Int J Radiat Oncol Biol Phys. **35(2)**: 383-397 (1996). doi:10.1016/0360-3016(96)00084-3

[33] N. Hu, M. Nakao, S. Ozawa et al., Application of Stoichiometric CT Number Calibration Method for Dose Calculation of Tissue Heterogeneous Volumes in Boron Neutron Capture Therapy. Med. Phys. **51**, no. 6: 4413-4422. Accessed November 1, (2024). doi:10.1002/mp.17093

[34] G. Leunens, J. Verstraete, A. Dutreix et al., Assessment of dose inhomogeneity at target level by in vivo dosimetry: can the recommended 5% accuracy in the dose delivered to the target volume be fulfilled in daily practice? Radiother Oncol. **25(4)**: 242-250 (1992). doi:10.1016/0167-8140(92)90243-N

[35] International Commission on Radiation Units and Measurements, *Determination of absorbed dose in a patient irradiated by beams of X- or gamma-rays in radiotherapy procedures*.(Report 24, ICRU Publications, Washington DC, 1976).